INFLUENCE OF GRID FINGER AND BUS BAR STRUCTURE ON THE PERFORMANCE OF REAR-LINE-CONTACTED SILICON CONCENTRATOR CELLS

A. Mohr, M. Hermle, T. Roth, S. W. Glunz
Fraunhofer Institute for Solar Energy Systems ISE
Heidenhofstrasse 2, 79110 Freiburg, Germany
Phone: ++49 761 4588 5148, Fax: ++49 761 4588 9250, Email: andreas.mohr@ise.fraunhofer.de

ABSTRACT: Silicon concentrator solar cells used in high concentrator systems (up to 500x) have a high potential to achieve cost reduction for solar generated electricity. Many different small-sized (4.5 mm x 4.5 mm) rear-line-contacted concentrator cells (RLCC), all integrated in one single wafer, were fabricated. These cells are designed for application in an one–axis tracking linear concentrator system with dielectric compound parabolic concentrators second stage. The best cell reaches a maximum efficiency of 24% at 63 suns and has a high performance under high concentration (23.2% at 265x). Experimental results show that the grid finger distance and especially the position of the bus bars influence strongly the performance of these cells. A two-dimensional model for these concentrator cells is presented and numerical simulations results are discussed.
Keywords: Back contact, c-Silicon, Concentrator Cell

1 INTRODUCTION

At Fraunhofer ISE small-sized silicon concentrator cells for application in a linear one-axis tracking concentrator system achieving a high geometrical concentration of 300x are under development. The concentrator system consists of a parabolic mirror trough used as first stage and compound parabolic concentrators (CPCs) as second stage, which are optimised for concentrating the sun light by total internal reflection. The system is tracked around a polar oriented axis and the mirror focuses the light (39.7x) onto a row of dielectric non-imaging 3D-CPCs, concentrating the sun light up to 7.7x [1-3].

For this concentrator system rear-line-contacted concentrator cells (RLCC) with an active cell area of 4.5 mm x 4.5mm matching with the exit area of the CPCs will be used. These cells are optimised for high concentration (>200x) having linear oxide openings on the rear side for low recombination losses at the contacts and for avoiding current crowding and contact resistivity problems under high-level injection.

To find an optimum rear-contacted cell structure we designed a set of masks for processing 85 different concentrator cells on one single four-inch FZ wafer [4,5]. The following parameters of these 85 concentrator cells are varied: Distance of the grid fingers, width of oxide openings, width of diffused areas, finger type (tapered and not tapered), distance of the non-metallised regions on the rear side, bus bars inside and outside of the active cell area .

Measurement results and simulations show a strong influence of the grid fingers and the position of the bus bars on the cell performance. The smaller the grid distance the higher is the concentration at which the efficiency of the cell peaks. Bus bars lying inside the active cell area decrease strongly the cell performance in contrast to cells having bus bars outside the active cell area.

In order to simulate our rear-line-contacted concentrator cells we have developed a 2-dimensional numerical model. The ray-tracing program *RAYN* and the numerical device simulators *MESH* and *DESSIS* [6] are controlled by the simulation environment *PVObjects* [7].

This paper describes our 24% efficient rear-line-contacted silicon concentrator (RLCC) cell, analyses the limitations of the cell performance due to the metallisation structure and points out how to overcome these limitations in order to improve the RLCC cell efficiency.

2 CELL DESIGN

The design of our rear-line-contacted concentrator cell is shown in Figure 1.

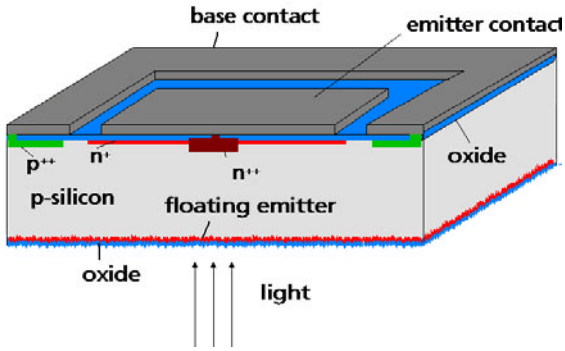

Figure 1: Rear-line-contacted silicon concentrator cell (RLCC).

On the front side the cell is textured with random pyramids in order to reduce reflection and to increase the absorption. The n-doped floating emitter on the front side is passivated by a thermal antireflection oxide reducing the surface recombination. The cells were processed on 1 Ω cm p-doped FZ base material. On the rear side a large fraction is covered by a shallow emitter simultaneously diffused with the front emitter which serves as the active junction. Local deep phosphorus and boron diffusion lines underneath both the emitter and the base contacts, respectively, reduce the contact resistivity and recombination. Due to the resulting high surface doping concentration it is possible to use Ti/Pd/Ag not only for the emitter but also for the base contacts. The active area of these cells is 4.5 mm x 4.5 mm matching with the exit area of the CPCs. The chip size of the cells after cutting out of the wafer accounts 7.5 mm x 7.5mm but will be reduced in future cell designs.

3 MEASUREMENT RESULTS AND SIMULATIONS

In the following the influence of the grid finger distance and of the bus bar position (inside or outside the active cell area) on the cell performance will be described. We also present and discuss the measurement results of our best cell reaching a maximum efficiency of 24% at 63 suns and a high performance of 23.2% at 265x.

3.1 Variation of grid finger distance

The measurement of efficiency versus incident power for different grid finger distances between a p- and n-finger are shown in Figure 2. The corresponding cell parameters are listed in Table I. The unmetallised spacings between a p- and n-finger is kept constant at 50 µm for all cells. The oxide openings are always 9% of the n- to n-finger distance. The width of the deep diffusion underneath both the emitter and the base contacts and the width of the shallow emitter diffusion is adapted to the oxide openings given in Table I. Therefore the cell performance depends mainly on the different grid finger distances. The cells are fabricated on 1 Ω cm p-doped FZ material and all cells are 130 µm thick. The height of the metallisation is 3 µm using lift off technique. Main cell results are presented in Table II.

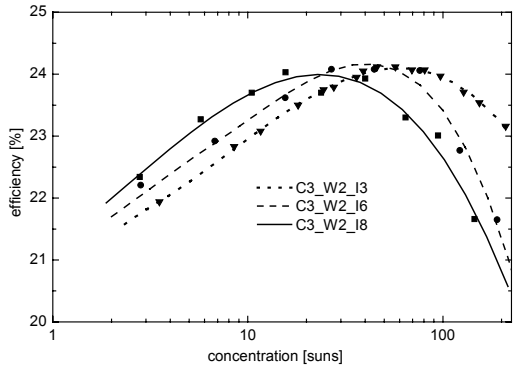

Figure 2: Variation of the grid finger distance resulting in different peak efficiencies at different concentrations.

Figure 2 shows that the cell efficiency peaks for smaller grid distances at higher concentrations. This is particularly effected by shorter lateral carrier diffusion in the base due to smaller grid finger distances. A shorter lateral carrier diffusion path results in lower series resistance leading to higher FF under high concentration.

Table I: Cell parameters of the presented RLCC cells.

Cell C3_W2_	I3	I6	I8
Distance n-to n- finger[µm]	201.8	310	387.5
Oxide openings [µm]	18	28	35

FF losses are the reason why the cell efficiency of C3_W2_I3 peaks at 62x, of cell C3_W2_I6 at 38x and of cell C3_W2_I8 at 23x although all cells reach the same maximum efficiency of around 24% and a FF of around 82% at their peak concentrations. Thus for application of the RLCC cell in concentrator systems above 200x the grid finger finger distance has to be as small as technologically possible in order to overcome high series resistance losses.

Table II: Measurement results for peak concentration and for high concentration at 200x.

Cell C3_W2_	I3	I6	I8
Concentration	62x	38x	23x
FF [%]	82	82.3	81.9
Eta [%]	24.1	24.2	24
R_s [Ω cm^2]	0.011	0.019	0.023
Concentration	200x	200x	200x
FF [%]	77.3	70.9	68.2
Eta [%]	23.2	21.4	20.8

3.2 Comparison of bus bar position inside and outside of the active cell area

The active cell area of our concentrator RLCC cells is 0.2025 cm^2 matching with the exit area of the CPCs of the linear concentrator system. For an easy mounting and electrical connection on a cell receiver the p- and the n-bus bars are 0.8 mm x 4.5 mm placed on the rear side of the cell. In order to integrate as many cells as possible on a four-inch FZ wafer both bus bars of some cells are integrated inside of the active cell area. On one wafer 220 RLCC cells instead of 164 cells could be processed if the bus bars are inside instead of outside of the active cell area. The integrated bus bars have line contacts to work like an additional finger. Underneath the n-bus bar contact local deep n^{++}-diffusion is used for a low contact resistance. In order to reduce the risk of shunting through the oxide layer and to collect generated carriers, a shallow n^{+}-diffusion is underneath the n-bus bar and a deep p^{++}-diffusion is underneath the p-bus. Measurement results of cells processed on a 1 Ω cm p-doped wafer and only differing in the position of the bus bars are shown in Figure 3. Placing the bus bars into the active cell area obviously reduces the efficiency strongly.

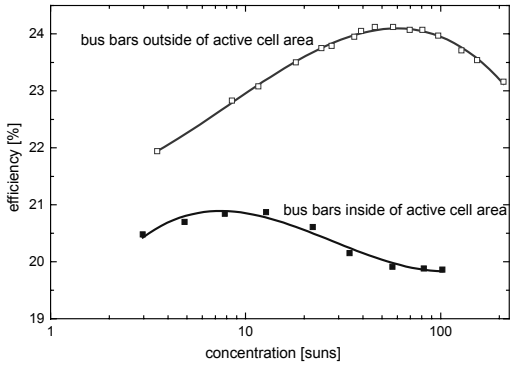

Figure 3: Measurement results of cells only differing in the position of the bus bars.

For a detailed investigation of these results we developed a two-dimensional model for our RLCC cells. We performed *DESSIS*-simulations for three different symmetry elements with bulk doping of 1 Ω cm. The elementary diode describes the cell area between the two bus bars, the n- and p–busbar diodes describes the corresponding areas under the bus bars. In a network circuit we interconnected the IV-curves of the three diodes to obtain the IV-curves of the entire cell. The resulting fill factors of the device simulations and the

circuit simulations are shown in Figure 4.

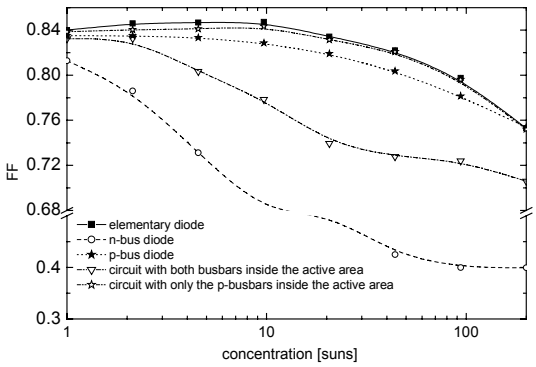

Figure 4: Simulation results of the different device simulations and the circuit simulations.

The simulations show, that the fill factor of the n-bus diode element decreases much stronger (note to the break in the y-axis) as the fill factor of the elementary diode and the p-bus bar diode. This is leading to a strong impact of the fill factor of the entire cell, as the results of the circuit simulations with both bus bars inside the active area show. If only the p-bus bar is inside the active area, the fill factor loss in the entire cell is negligible, as can be seen in Figure 4.

In order to investigate the differences of the two bus bar diodes, we have compared the current flow pattern in the areas above the bus bars. Figure 5 and 6 show the two-dimensional plots of the hole current density of the n-bus bar and the p-bus bar diode respectively.

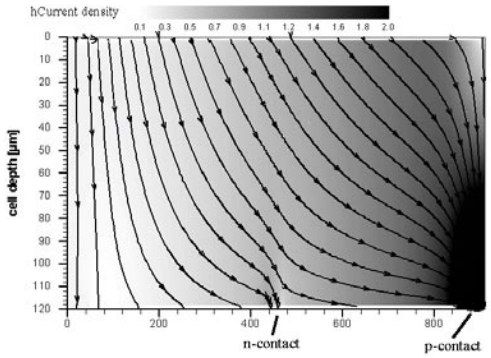

Figure 5: Two-dim. plot of a simulated n-bus bar element. Arrows show the flow of the majorities (holes). Current crowding problems at the p-contact decrease the FF. The shallow n^{+}-diffusion of the n-bus bar reaches from 50 µm to 850 µm.

Underneath the n-bus bar (Figure 5) high current crowding of the majorities (holes) at the p-contact leads to the decrease of the FF. This is due to the high amount of carriers which have to be collected from the region under the n-bus. Underneath the p-bus bar the majorities diffuse directly to the collecting deep p^{++}-diffusion so that the FF losses could be neglected.

If both bus bars are within the illuminated area mainly the characteristic of the n-bus bar is leading to the high efficiency losses as shown in Figure 3 and 4. To avoid these losses it is only necessary to put the n-bus bars outside the active area.

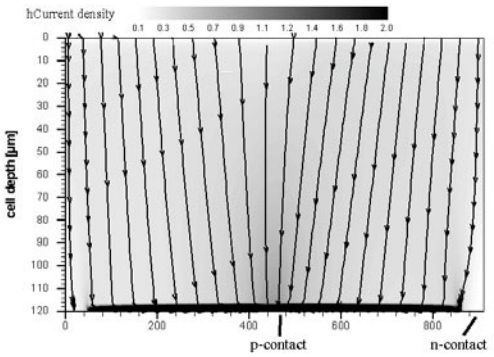

Figure 6: 2-dim. plot of a simulated p-bus bar element. Majority flow is indicated by the arrows. The majorities diffuse directly to the collecting p^{++}-diffusion. The deep p^{++}-diffusion of the p-bus bar reaches from 50 µm to 850 µm.

3.3 24% rear-line-contacted silicon concentrator cell

So far our best cell is fabricated on 1 Ω cm p-type FZ material. The efficiency and the FF versus concentration is shown in Figure 7. This RLCC cell has the smallest grid finger distance between a n-and n-finger (201.8 µm) and the smallest unmetallised spacing (50 µm) between two fingers we have produced so far. The bus bars lie outside of the active cell area in order to avoid FF losses as described in chapter 3.2. This RLCC cell reaches a maximum efficiency of 24% at 63x and still has an high efficiency of 23.2% and a FF of 77.7% at 265x.

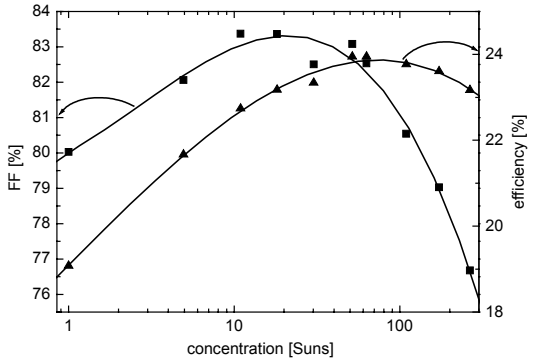

Figure.7: The best RLCC silicon cell

Table III: Performance of best RLCC cell fabricated so far

Conc.	V_{oc}[mV]	I_{sc}[mA]	FF [%]	Eta [%]
63x	773.7	447.5	82.5	24.0%
265x	805.6	1885.3	77.7	23.2%

The plot of V_{oc} of our best cell versus the logarithm of incident intensity is shown in Figure 8. V_{oc} increases not linearly but sublinearly with increasing logarithm of the concentration. This effect can be explained by the transition from SRH bulk recombination under low level injection conditions to Auger recombination under high level injection ($n = p >> N_b$). Figure 8 shows the decrease of the ideality factor n with increasing concentration. The ideality factor n of the one sun diode model is an indicator for the different recombination processes shown in Table IV. In order to determine n in dependence of the incident intensity we interpolated the V_{oc} graph versus the logarithm of C with a polynomial of

second order. The derivation of this fit versus the logarithm of C gives the ideality factor n as derived and implied by Equation (1) to (3).

$$J \approx J_0 e^{\frac{V - JR_s}{V_T n}} - CJ_{ph}^1 \quad (1)$$

where $V_T = \frac{kT}{q}$

and J_{ph}^1 is approximate the one-sun short circuit current under standard test conditions.

Therefore V_{oc} becomes

$$V_{oc}(C) \approx V_T \ln \frac{CJ_{ph}}{J_0} \approx V_{oc}^1 + nV_T \ln C \cdot \quad (2)$$

whereas V_{oc}^1 is the V_{oc} at 1 sun under STC.

From equation (2) follows

$$n = \frac{q}{kT} \frac{\Delta V_{oc}}{\Delta \ln(C)} \cdot \quad (3)$$

A decrease of the ideality factor n below n = 1 with increasing concentration is visible in Figure 8 and n approximates to the theoretical limit of 2/3 for dominating Auger recombination in the highly injected case. That means for our rear-line-contacted concentrator cell under low level injection the bulk SRH recombination dominates the cell performance, in the highly injected case Auger recombination starts dominating the cell performance. The transition from SRH bulk recombination to Auger recombination cause the sublinearity of V_{oc} versus the logarithm of concentration.

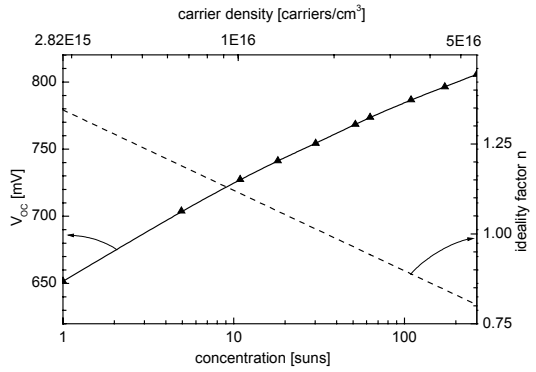

Figure 8: V_{oc} of cell C3_W2_I3 versus incident intensity.

Table IV: Ideality factors for different recombination processes under low and high injection.

Recombination process	Injection level	Ideality factor
Bulk-SRH	Low injection	1
	High injection	2
Emitter	Low injection	1
	High injection	1
Auger	High injection	2/3

V_{oc} of the RLCC cell at one sun is 20 to 30mV lower than the V_{oc} of a standard high efficiency solar cell. Simulations show that this degradation results not only from the larger oxide openings on the rear side but rather from passivation problems underneath the n grid fingers. Using aluminum instead of Ti/Pd/Ag may improve the passivation and the reflection leading to higher light trapping. For testing aluminum on the rear side new batches are running.

4 CONCLUSIONS AND OUTLOOK

For the one-axis tracking linear concentrator system of Fraunhofer ISE we are developing rear-line-contacted concentrator cells (RLCC).

The best cell reaches a maximum efficiency of 24% at 63 suns and shows high performance under high concentration (23% at 265x). In order to improve the cell performance the grid finger distance between a n- and p-finger has to be as small as technologically possible avoiding high FF at high concentration (>100x). For a high packing density of RLCC cells on an expensive four-inch FZ wafer cells with bus bars inside instead of outside of the active cell area were processed and investigated.

Simulations show that the measured efficiency losses if both bus bars integrated into the active area result from current crowding problems underneath the n-bus bar. In order to avoid these losses, it is possible to integrate the p-bus bar inside of the active cell area but it is necessary to put the n-bus bar outside of the active cell area.

The RLCC cell together with the one-axis tracking concentrator seems to be on the right way to be a low-cost and high-efficient concentrator module working at a concentration of around 230 suns.

ACKNOWLEDGEMENTS

This work was partly funded by the EC (Project N⁰:NNE5-2001-00207);

the authors also like to thank the clean room group of ISE Freiburg for supporting the cell fabrication.

REFERENCES

[1] M. Brunotte, A. Goetzberger, and U. Blieske, Solar Energy **56** (1996) 285-300.

[2] M. Hein, F. Dimroth, G. Siefer, and A. W. Bett, Solar Energy Materials & Solar Cells **75** (2003) 277-283.

[3] A. Mohr, T. Roth, and S. W. Glunz, Proceedings of the 19th European Photovoltaic Solar Energy Conference, Paris, France (2004) to be published.

[4] T. Roth, A. Mohr, and S. W. Glunz, Proceedings of the 19th European Photovoltaic Solar Energy Conference, Paris, France (2004) to be published.

[5] R. A. Sinton and R. M. Swanson, Proceedings of the 19th IEEE Photovoltaic Specialists Conference, New Orleans, Louisiana, USA (1987) 1201-1208.

[6] DESSIS Manual 7.0, (Zurich, 2001).

[7] J. O. Schumacher, PhD Thesis, University of Konstanz, 2000.